generated in this study will be made available on request, but may require a completed materials transfer agreement signed with Vir Biotechnology Inc. or the University of Washington.

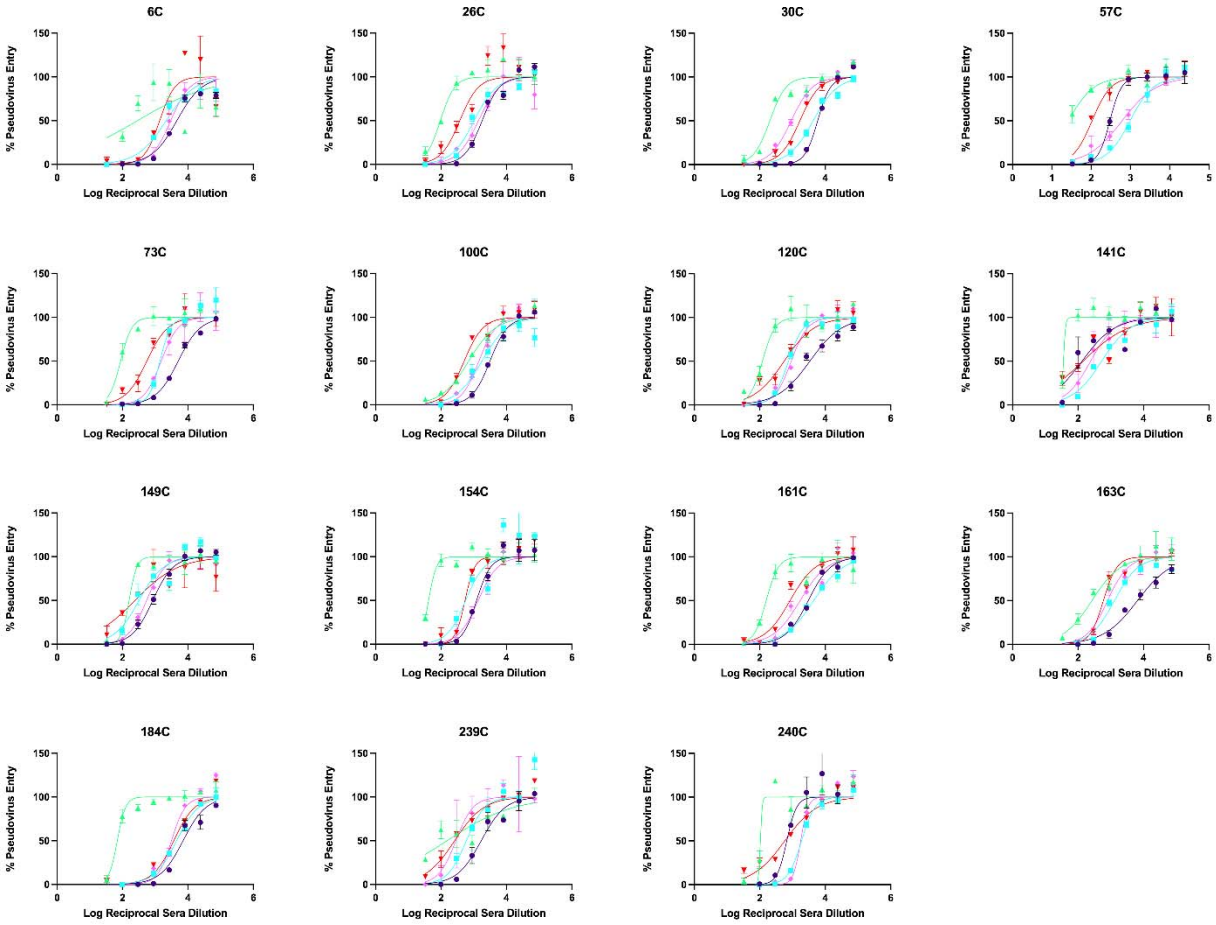

Fig. S1A: Infected-vaccinated plasma VSV neutralization curves. Purple shows G614, Teal is Delta, Red is Omicron BA.1, Light Pink is Omicron BA.2, and Green is SARS-CoV.

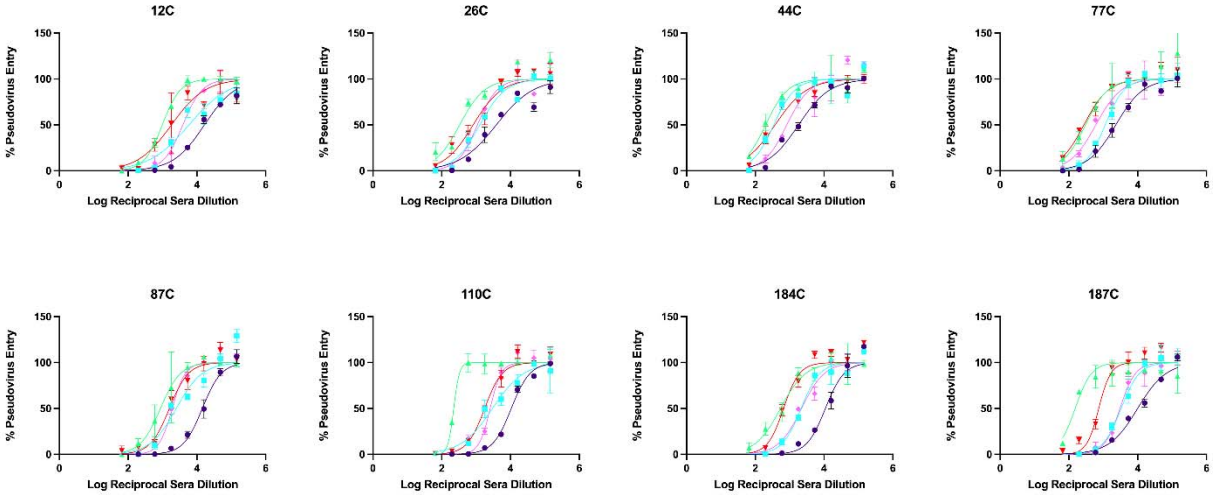

Fig. S1B: Delta breakthrough plasma VSV neutralization curves. Purple shows G614, Teal is Delta, Red is Omicron BA.1, Light Pink is Omicron BA.2, and Green is SARS-CoV.

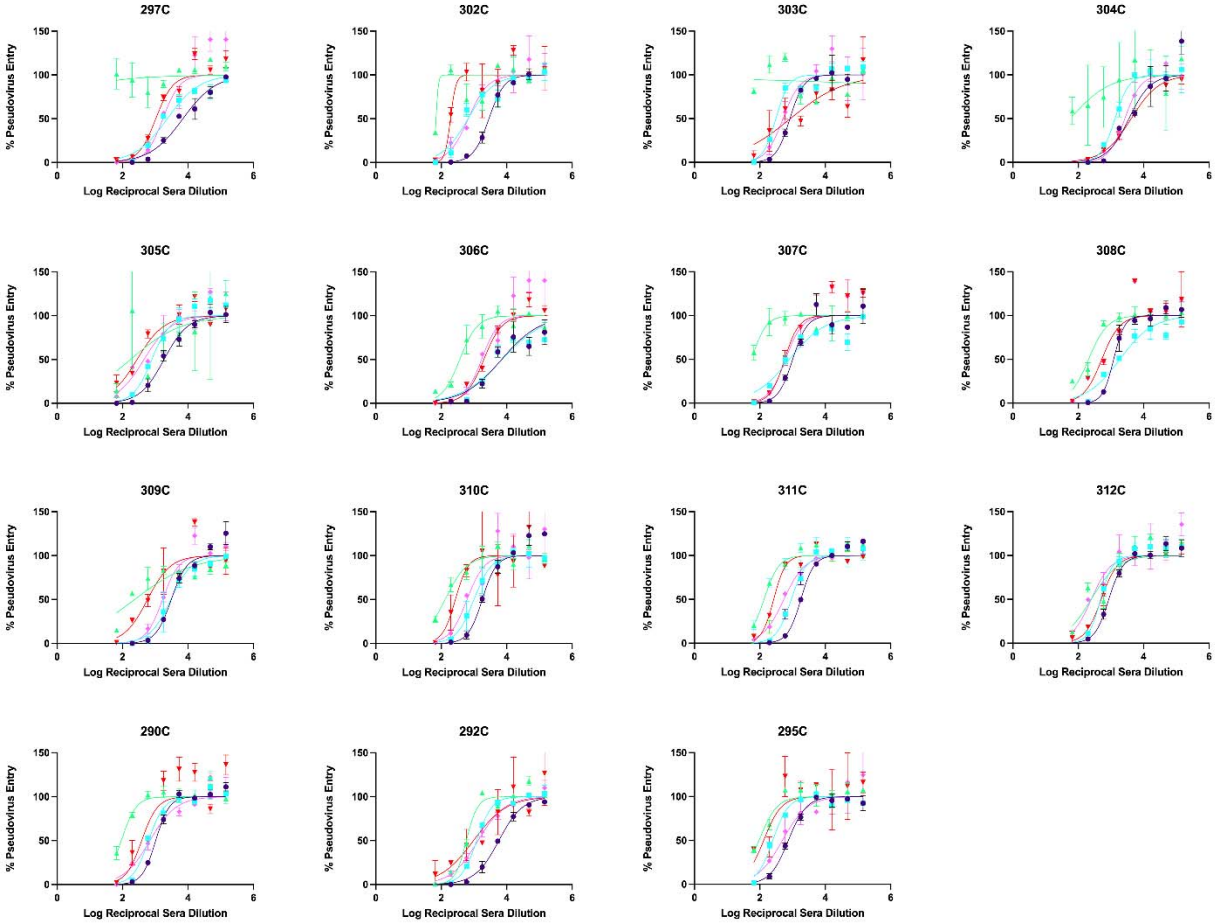

Fig. S1C: Omicron BA.1 breakthrough plasma VSV neutralization curves. Purple shows G614, Teal is Delta, Red is Omicron BA.1, Light Pink is Omicron BA.2, and Green is SARS-CoV.

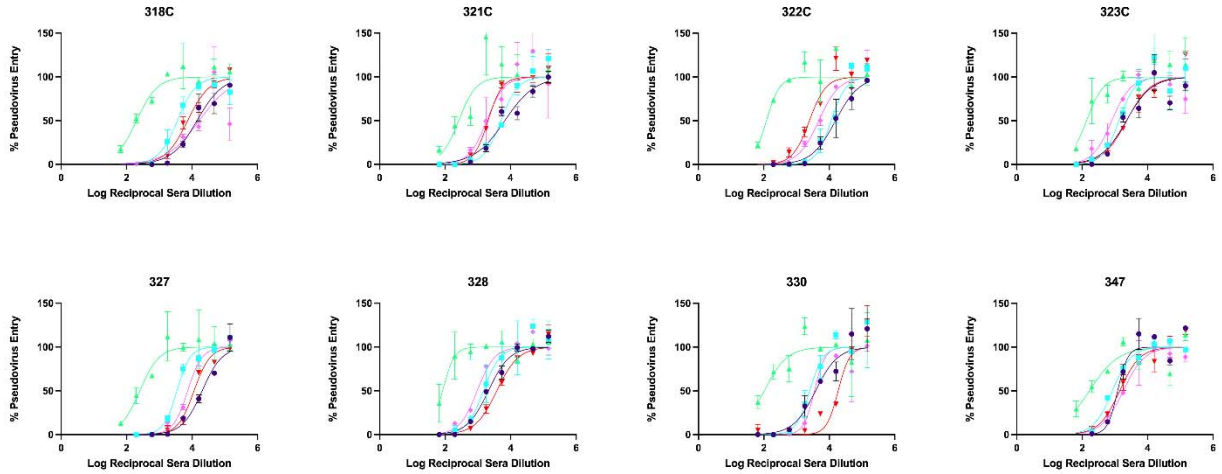

Fig. S1D: Infected-boosted plasma VSV neutralization curves. Purple shows G614, Teal is Delta, Red is Omicron BA.1, Light Pink is Omicron BA.2, and Green is SARS-CoV.

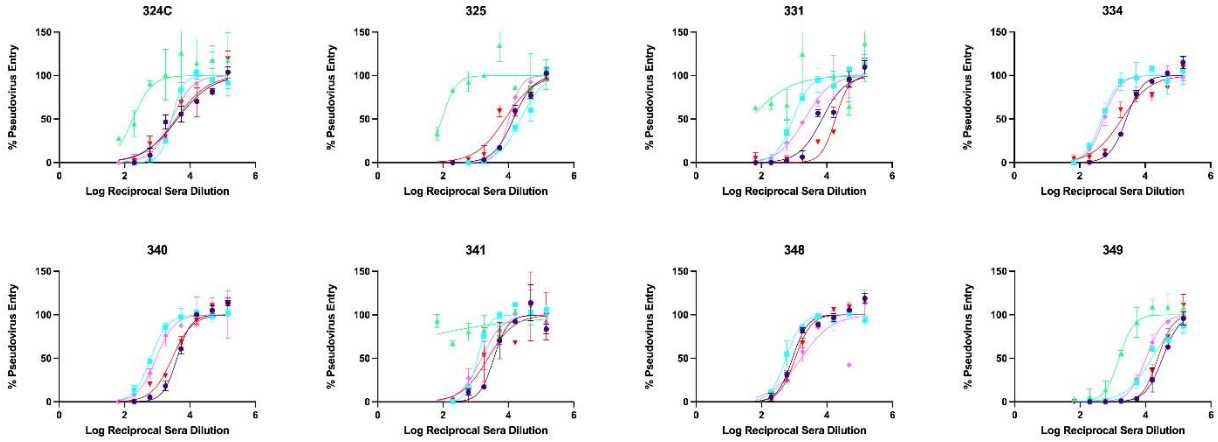

Fig. S1E: Vaccinated only-boosted plasma VSV neutralization curves. Purple shows G614, Teal is Delta, Red is Omicron BA.1, Light Pink is Omicron BA.2, and Green is SARS-CoV.

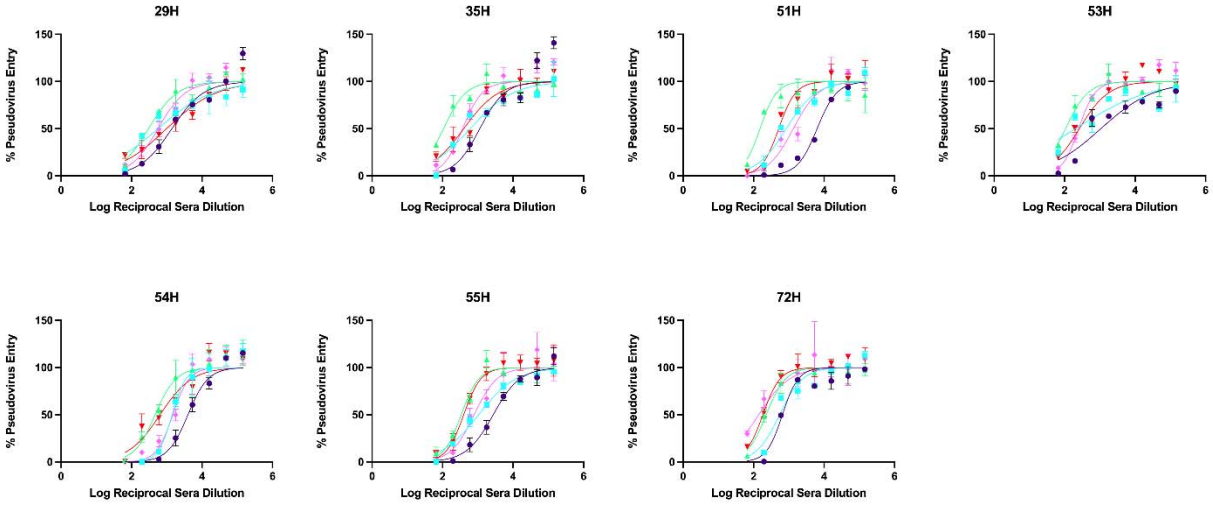

Fig. S1F: Omicron BA.1 breakthrough boosted plasma VSV neutralization curves. Purple shows G614, Teal is Delta, Red is Omicron BA.1, Light Pink is Omicron BA.2, and Green is SARS-CoV.

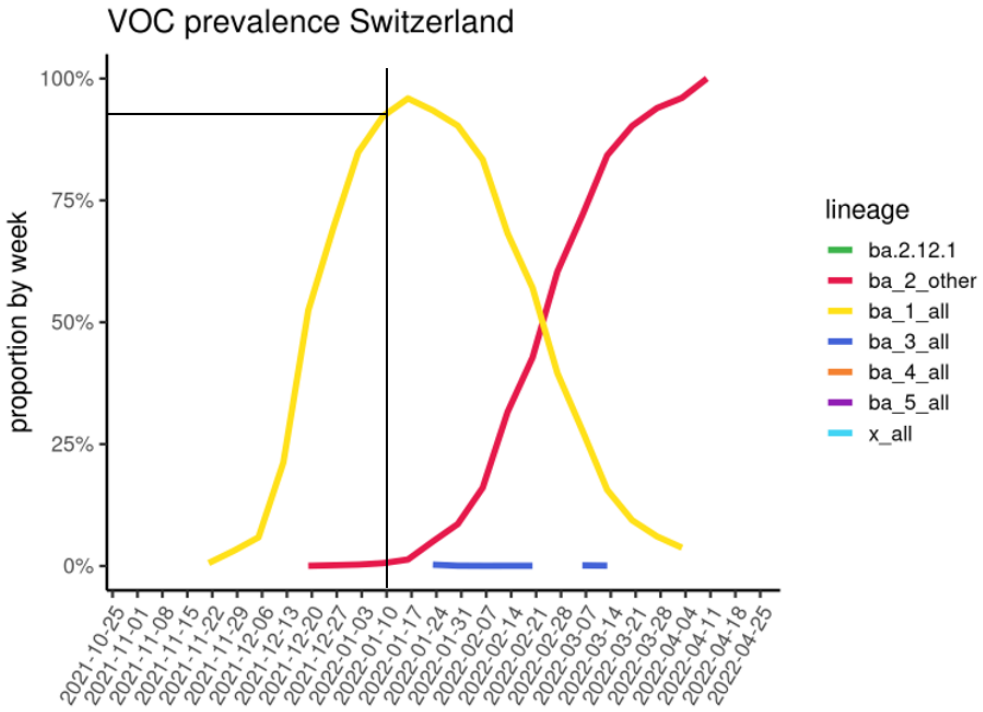

Fig. S2. Variant prevalence in Switzerland at the end of 2021 and early 2022

Data S1. Description of the Cohorts of SARS-CoV-2-immune, vaccinated, or hybrid individuals, Related to Figure 1A, E-F (External PDF)

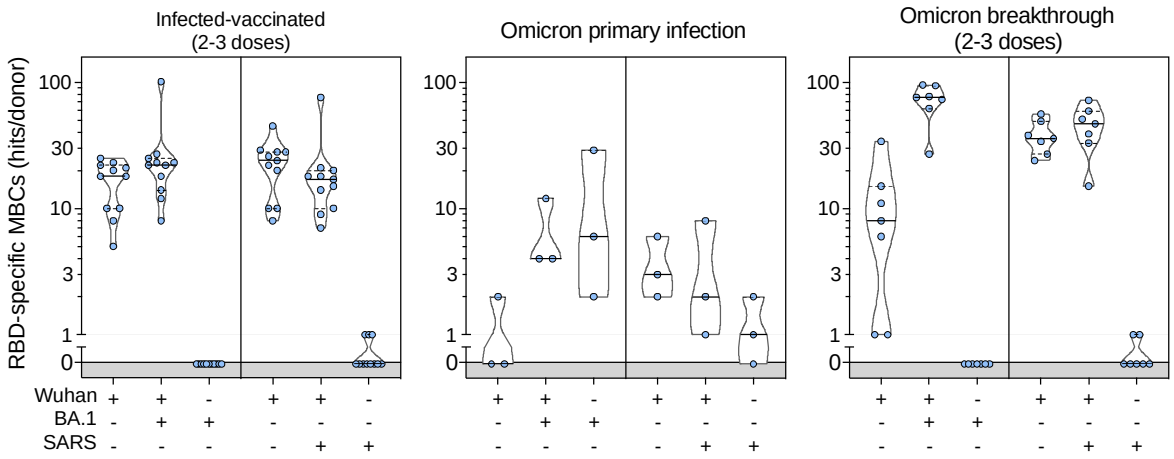

Fig. S3. Cross-reactivity of IgGs secreted from memory B cells obtained from infected-vaccinated individuals (left, n=11), subjects who experienced a primary infection with Omicron (center, n=3) or a breakthrough infection in January-March 2022 (right, n=7). Individual dots correspond to number of positive hits as shown in Fig. 1B relative to individual donors.

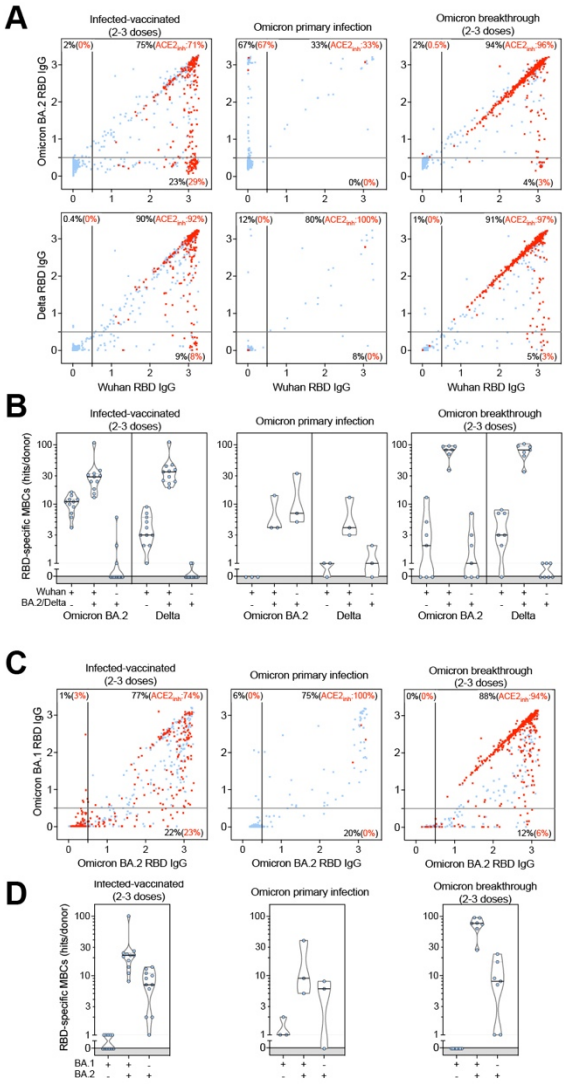

Fig. S4. Cross-reactivity of IgG antibodies derived from memory B cells. Antigen-specific memory B cell repertoire analysis (AMBRA) on PBMC obtained from infected-vaccinated individuals (left, n=11), primary SARS-CoV-2 infection (center, n=3) or breakthrough cases (right, n=7) occurring in January-March 2022 (Table S2). (**A** and **C)**, Each dot represents a well containing oligoclonal B cell supernatant screened for the presence of secreted IgGs binding to SARS-CoV-2 Wuhan-Hu-1 and BA.2 RBDs or Wuhan-Hu-1 and Delta RBDs using ELISA (A). A similar analysis on the same samples for the presence of secreted IgGs binding to the SARS-CoV-2 BA.1 and BA.2 RBDs (C). Red dots indicate inhibition of the interaction with ACE2 (using Wuhan-Hu-1 target antigen) as determined in a separate assay (Fig. S5). Percentages are relative to the total of positive hits against any of the antigen tested. **(B** and **D)**, Number of positive hits in panels (A, C) relative to individual donors.

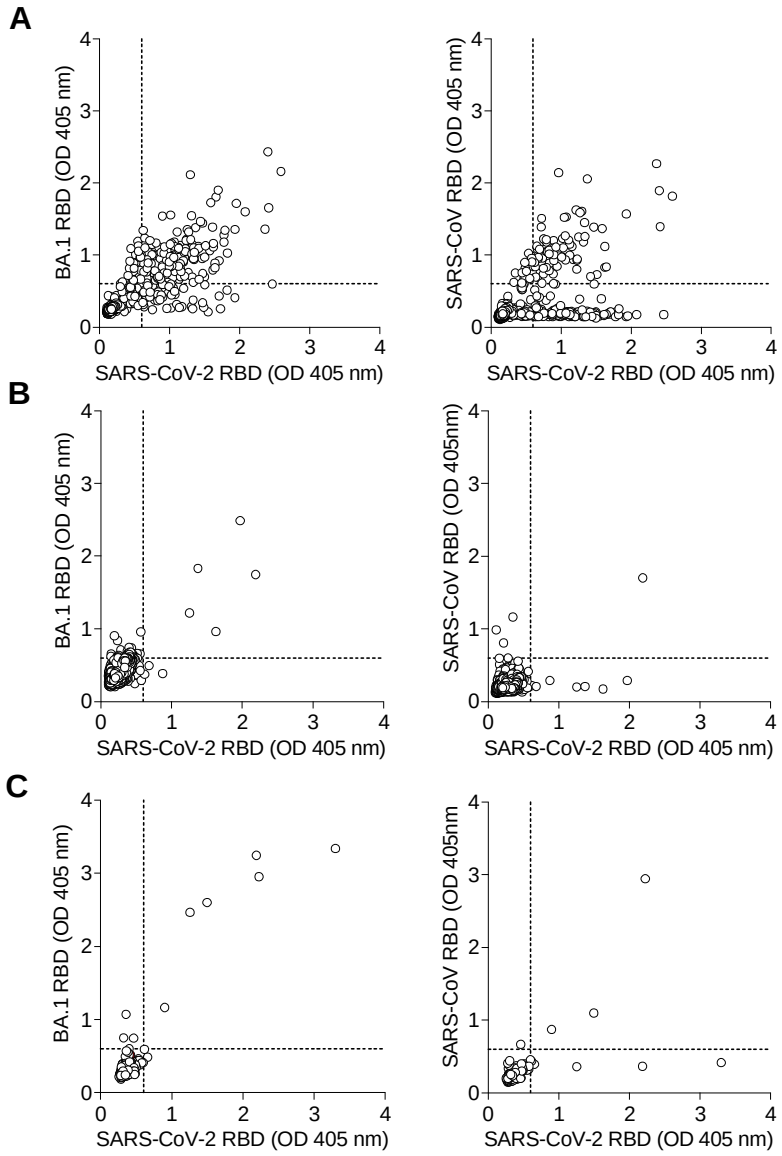

Fig. S5. Cross-reactivity of antibodies obtained from single-plasma cell cultures. Circulating CD138+ cells isolated from 3 vaccinated donors (A to C) approximately 1 week after Omicron breakthrough infection and cultured at 0.5 cells/well for 3 days. Culture supernatants were tested by ELISA for the presence of IgG binding to the SARS-CoV-2 Wuhan-Hu-1, BA.1 and SARS-CoV RBDs. Each dot represents the optical density (OD) values of individual cultures for each antigen tested.

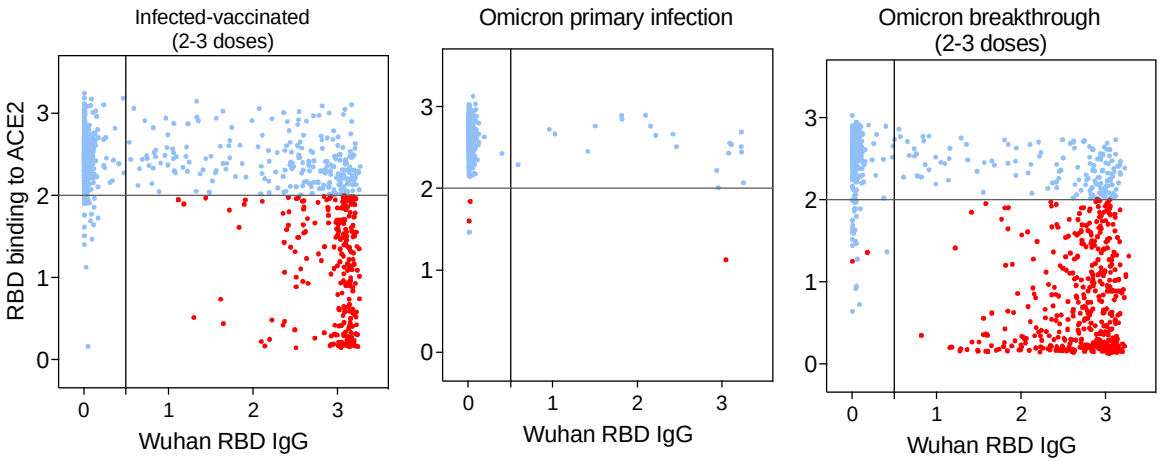

Fig. S6. Inhibition of RBD binding to human ACE2 by memory B cell-derived secreted antibodies. Antibody-mediated inhibition of SARS-CoV-2 Wuhan-Hu-1 RBD binding to solid phase ACE2 in function of IgG binding to matched RBD, as determined by ELISA. Each dot represents the optical density (OD) values of individual cultures. Red: cultures with antibodies inhibiting ACE2 binding to the RBD (as defined by a y-axis cutoff of OD≤2)

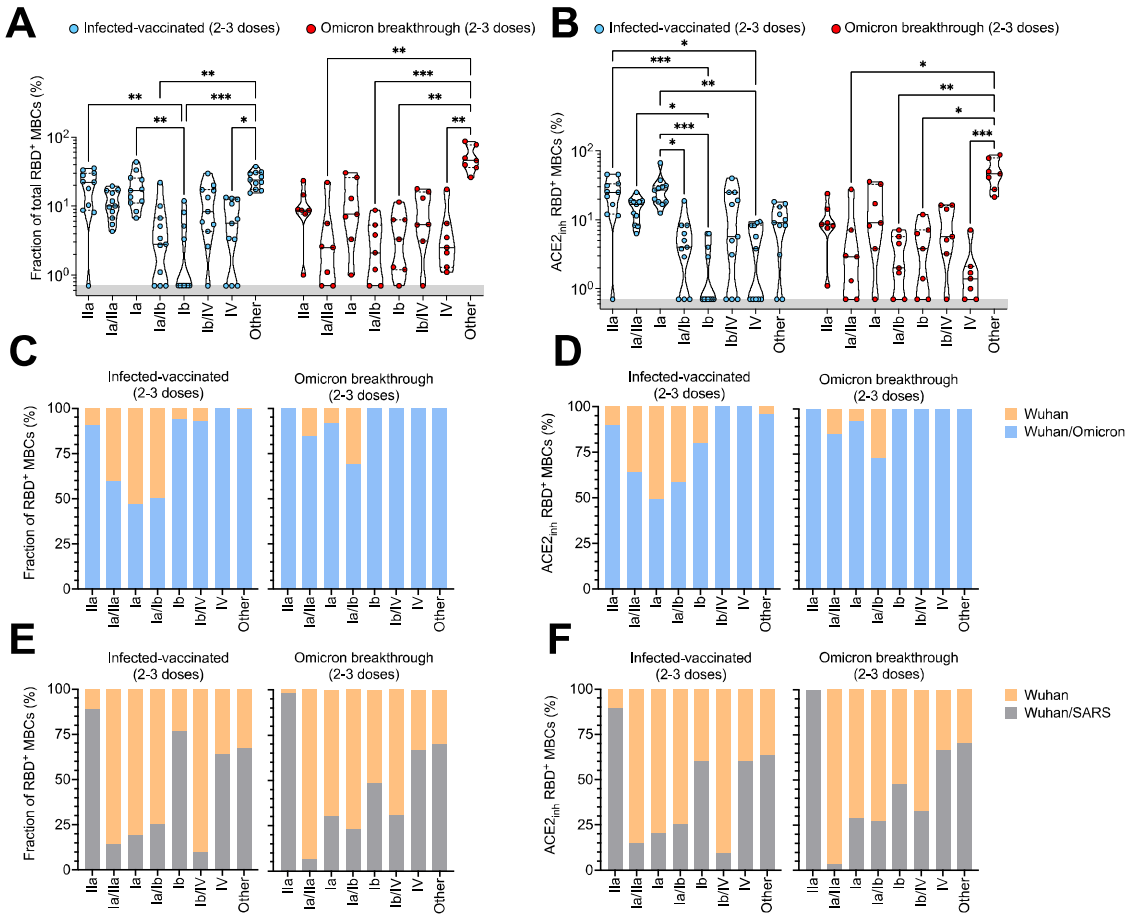

Fig. S7. RBD site definition and frequency analysis of IgG antibodies derived from memory B cells. RBD sites targeted by IgG derived from memory B cells were defined by a blockade-of-binding assay using monoclonal antibodies specific for sites Ia (S2E12), Ib (S2X324), IIa (S2X259) and IV (S309). Hybrid sites Ia/IIa, Ia/Ib and Ib/V were also defined when block of binding was observed by both corresponding mAbs. Lack of blockade by probe mAbs is indicated as "Other". **A-F** Graphs show frequency of total RBD-specific IgGs (A, C, E) and those inhibiting binding of RBD to human. Violin plots (A, B) show percentages of site-specific IgGs in individual donors analyzed. Bars (C-F) show cumulative frequencies of site-specific IgG antibodies filtered for their binding to Wuhan-Hu-1, Omicron BA.1/BA.2 and SARS-CoV RBDs.

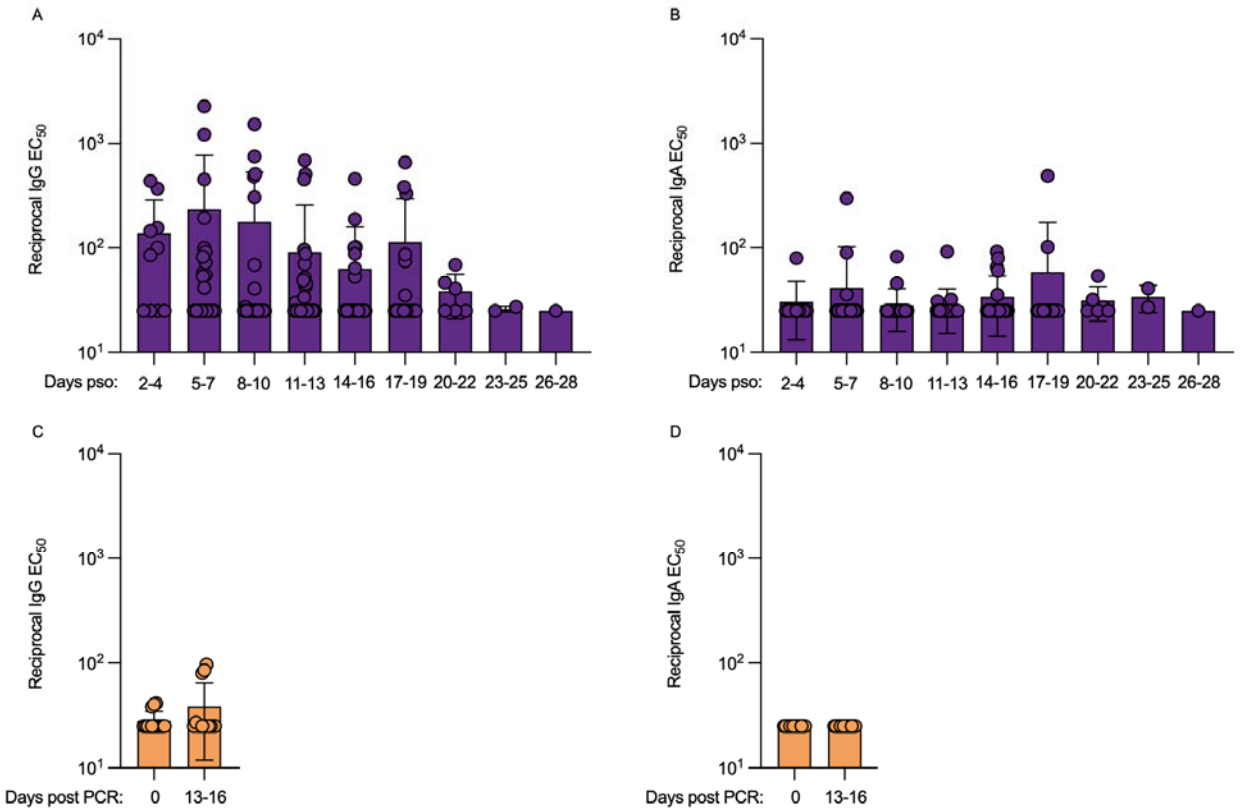

Fig. S8. IgG (A, C) or IgA (B,D) binding titers evaluated by ELISA (antigen: Wu-G614 S V-FLIP) in nasal swabs obtained longitudinally upon BA.1 breakthrough infection post symptom onset (pso, A,B) or in vaccinated-only individuals following a negative PCR test.

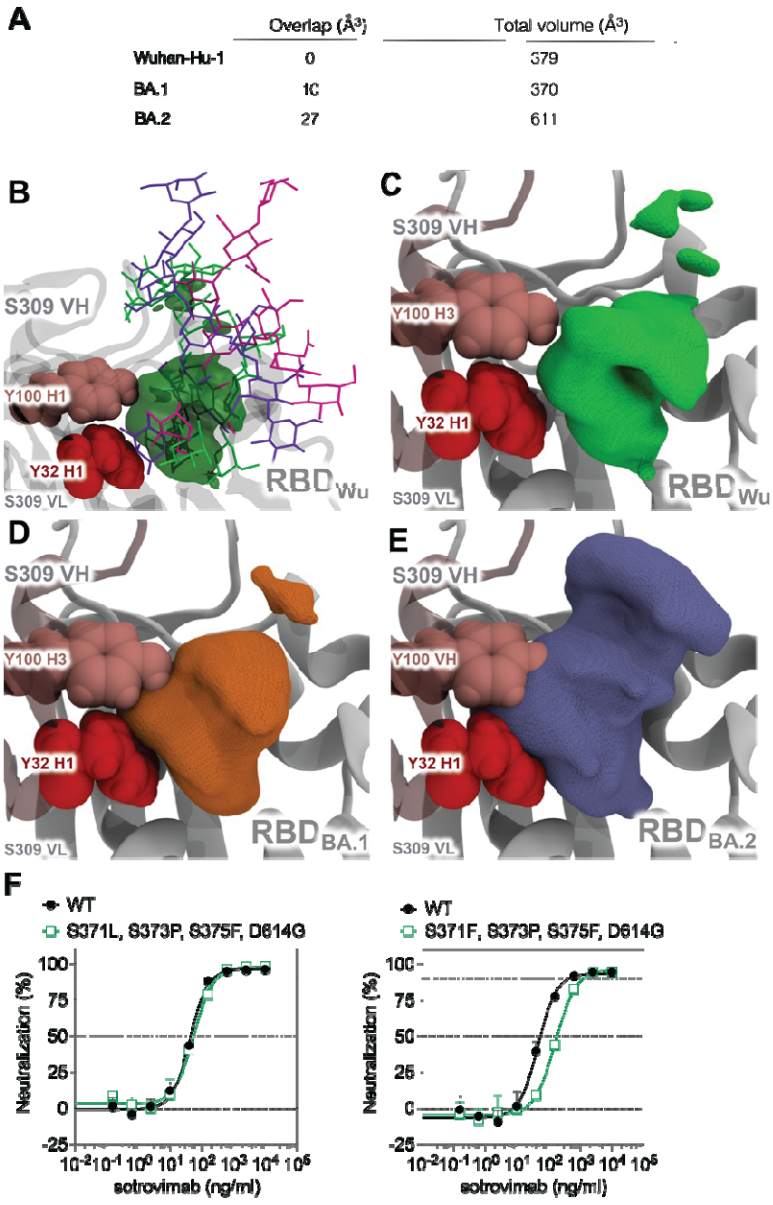

Fig. S9. BA.1 and BA.2 mutations impact the conformational preference of RBD glycans in MD simulations. (**A**) Summary of the overlap between the glycan and S309 volumetric density maps (Overlap) along with the total volume occupied by the glycan in the volumetric density map (Total volume). Volumetric density maps quantify the space occupied by the glycan with a maximum probability (isovalue) oS§f 0.057 (see Methods) during an MD simulation; smaller isovalues increase the volume size because ephemeral glycan conformations are included in the map whereas a larger isovalue reduces the volume size because only persistent glycan conformations are included in the map. (**B**) Overlay of three representative glycan conformations from MD of the RBD (Wuhan-Hu-1) shown as sticks, the volumetric map in translucent green, Y32 in H1 and Y100 in H3 as red spheres. (**C**) Volumetric density map of the glycan in RBD (Wuhan-Hu-1) is shown in green, the VH and VL of S309 is shown as a translucent cartoon, Y32 and Y100 in VH as spheres, and the RBD a grey cartoon. (**D**) Volumetric density map of the

glycan in RBD (BA.1) is shown in orange; otherwise depicted as in (**C**). (**E**) Volumetric density map of the glycan in RBD (BA.2) is shown in blue; otherwise depicted as in (**C**). Volumetric density maps are asymmetric because glycan dynamics are heterogeneous. (**F**) Neutralizing activity of sotrovimab against VSV pseudoviruses harboring the SARS-CoV-2 Wuhan-Hu-1 S (D614) with the indicated substitutions.

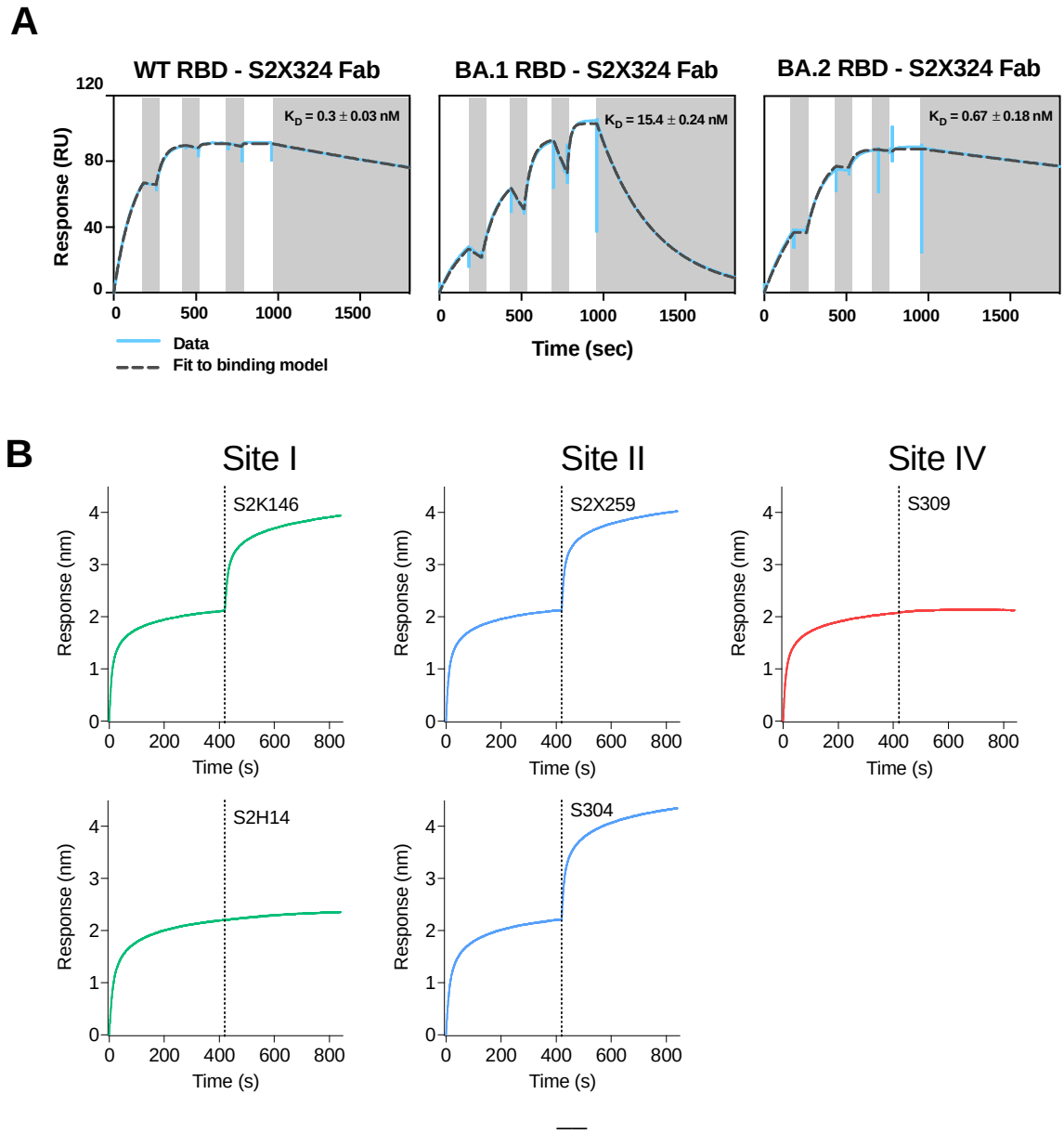

Fig. S10. Binding affinity and site specificity of S2X324 mAb (**A**) Binding of the S2X324 Fab to the SARS-CoV-2 Wuhan-Hu-1 (Wild-type, WT) RBD, Omicron (BA.1) RBD or Omicron BA.2 RBD immobilized at the surface of SPR chips. Experiments were performed with a 3-fold dilution series of Fab: 300, 100, 33, 11 nM and were run as single-cycle kinetics. (**B**) Competition binding assays for S2X324 versus site-I-targeting S2K146, S2H14; site-II targeting S2X259, S304; and site-IV-targeting S309 mAbs on SARS-CoV-2 RBD as measured by biolayer interferometry. One independent experiment out of two is shown.

A

mAb	Geomean IC50 (ng/mL) n≥2					
	WA1/2020	BA.1	BA.2	BA.4-V3G	BA.5	BA.2.12.1
sotrovimab	49.8	169.2	885.5	2650.7	1001.2	1896.7
S2X324	2.72	3.68	2.78	3.86	2.46	ND

mAb	Average fold change relative to WA1/2020 n≥2					
	WA1/2020	BA.1	BA.2	BA.4-V3G	BA.5	BA.2.12.1
sotrovimab	1.0	3.8	18.0	48.4	21.6	25.1
S2X324	1.0	1.3	1.0	1.5	0.9	ND

B

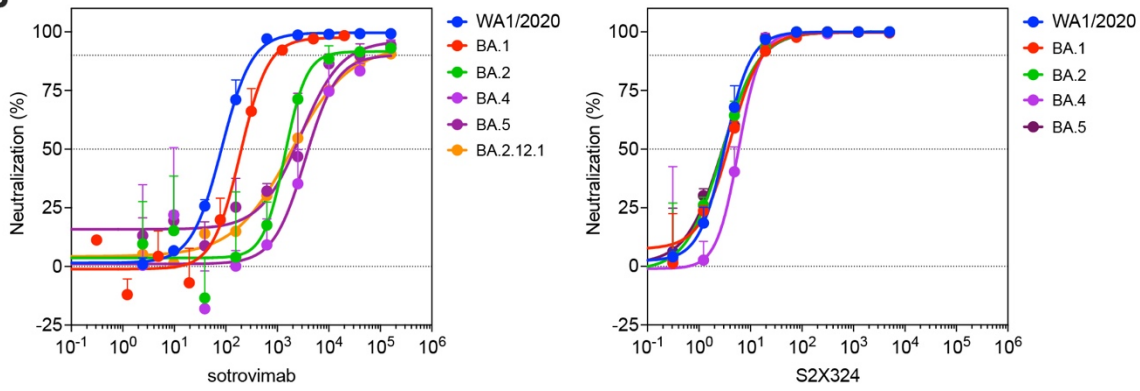

Fig. S11. Neutralization of authentic SARS-CoV-2 variants by sotrovimab and S2X324 (**A**) Geometric mean of IC50 values and average fold change for the neutralization of Omicron sublineages and WA1/2020 by sotrovimab and S2X324 mAbs. Strains tested: USA-WA1/2020; BA.1: hCoV-19/USA/MD-HP20874/2021; BA.2: hCoV-19/USA/MD-HP24556/2022: BA.4: hCoV-19/USA/MD-HP30386/2022; BA.5: hCoV-19/USA/COR-22-063113/2022; BA.2.12.1: USA/NY-MSHSPSPPV56475/2022 (B) Representative curves showing neutralization of SARS-CoV-2 strains by sotrovimab and S2X324. Data represent the means of triplicates ± standard deviation from one experiment. Omicron BA.1 data are reported from (*39*). Graph shown is representative of at least 2 independent experiments.

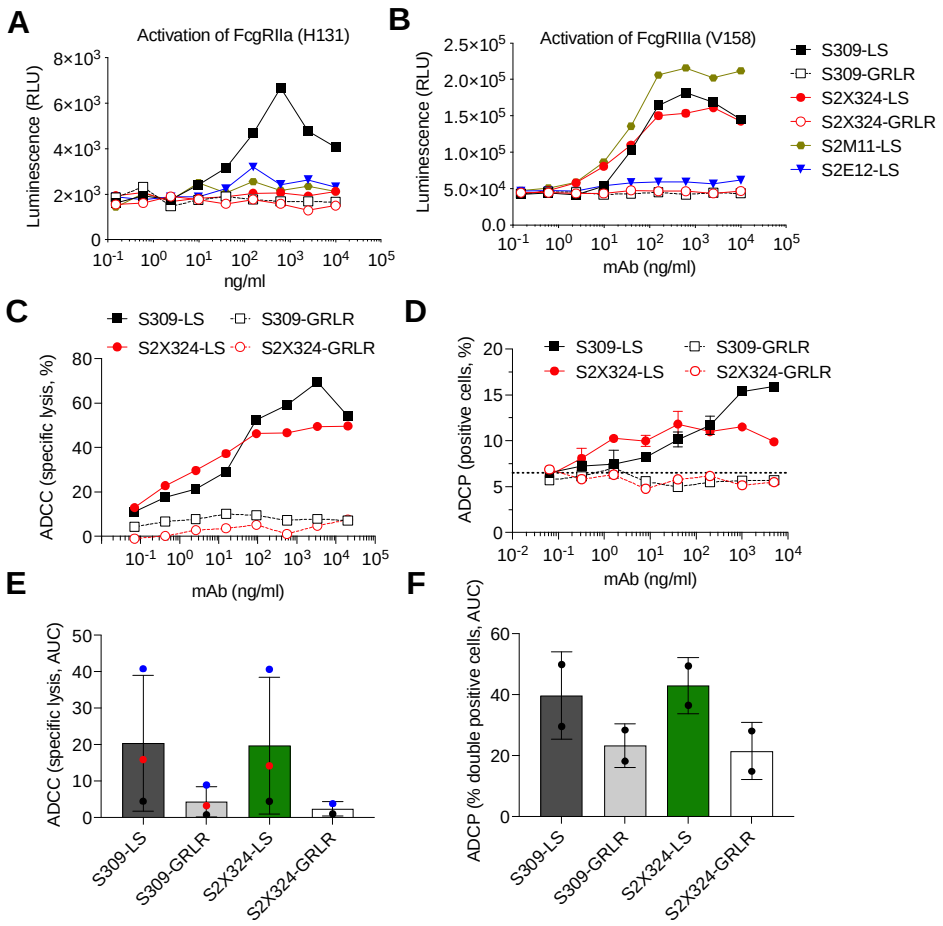

Fig. S12. In vitro effector functions by S2X324. (A-B), NFAT-driven luciferase signal induced in Jurkat cells stably expressing FcγRIIa H131 (A) or FcγRIIIa V158 (B) by S2X324 binding to prefusion stabilized SARS-CoV-2 Wuhan S stably expressed in ExpiCHO cells. SE12, S2M11, S309, S309-GRLR, S2X324-GRLR mAbs are included as controls (GRLR, Fc-null). **(C-E)** S2X324-triggered activation of ADCC (C, E) and ADCP (D, F) following incubation with PBMC and monocytes, respectively. AUC analyses of ADCC (**E**) and ADCP (**F**) mediated by S309-LS, S309-GRLR, S2X324-LS and S2X324-GRLR mAbs using primary NK cells or monocytes from three and two donors, respectively.

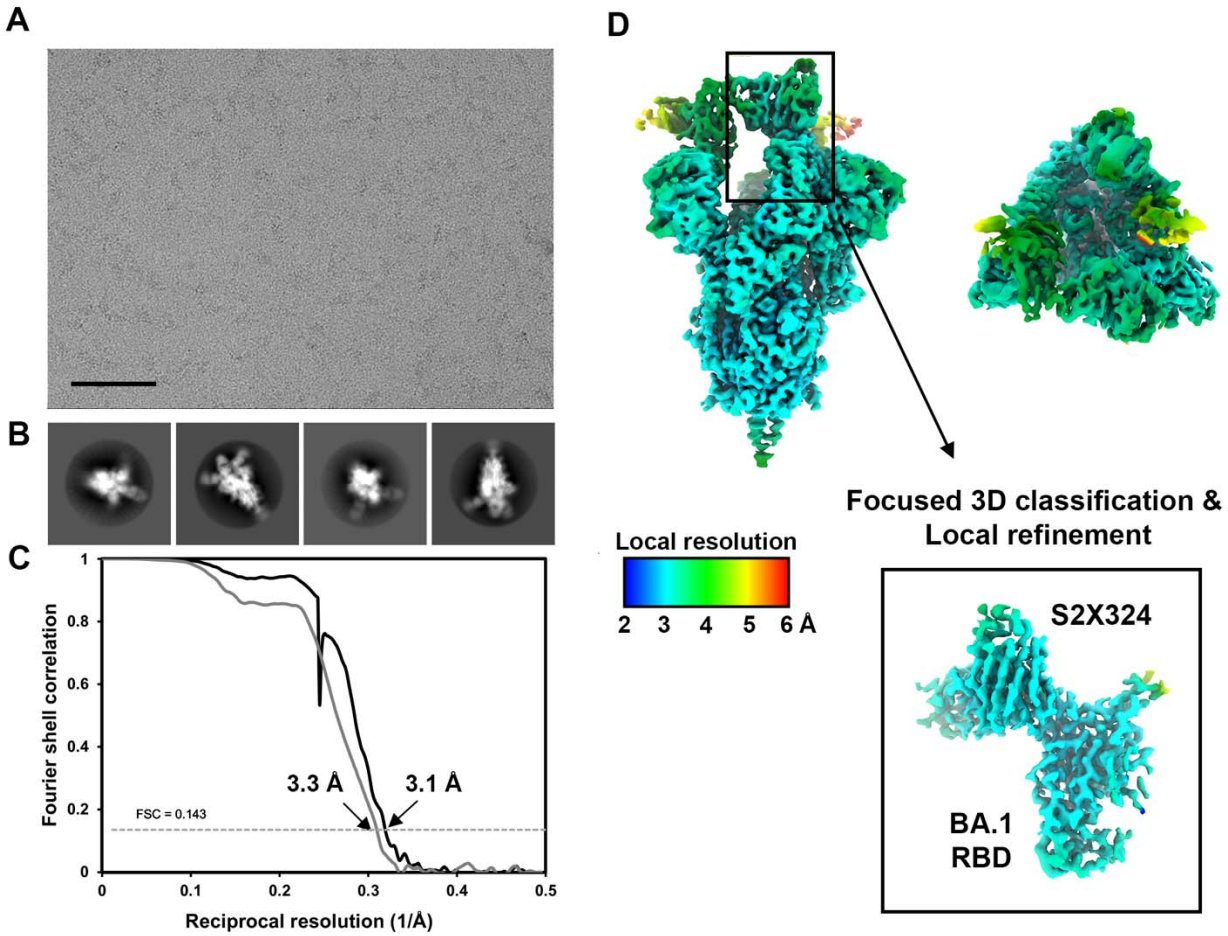

Figure S13. CryoEM data processing of the S2X324-bound SARS-CoV-2 Omicron BA.1 S dataset. A-B) Representative electron micrograph (A) and 2D class averages (B) of SARS-CoV-2 Omicron BA.1 S in complex with the S2X324 Fab embedded in vitreous ice. The scale bar represents 100 nm. **C)** Gold-standard Fourier shell correlation curves for the S2X324-bound SARS-CoV-2 S maps with two RBDs open state (black line) and locally refined RBD/S2X324 variable domain (grey line). The 0.143 cutoff is indicated by a horizontal dashed line. **D)** Local resolution maps calculated using CryoSPARC for the SARS-CoV-2 S/S2X324 Fab complex structure in two orthogonal orientations, the side view (left) and the top view (right) as well as for the locally refined RBD/S2X324 variable domain region (inset).

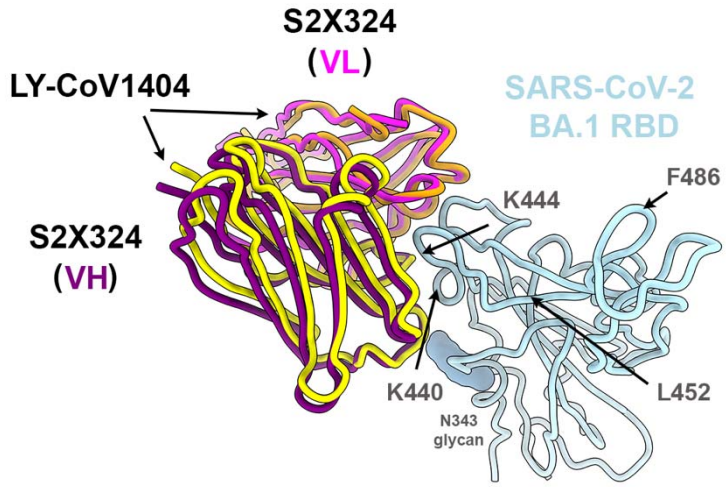

Figure S14. Superposition of S2X324 and LY-CoV1404 with RBD.
Ribbon diagram of LY-CoV1404/RBD structure (PDB 7MMO, yellow and orange) superimposed onto S2X324/RBD (CryoEM structure, purple and magenta), using the RBD as a reference. The N343 glycan is rendered as blue spheres. Two selected epitope residues and the BA.5 RBD mutation residues relative to BA.1, L452R and F486V, which are positioned outside the S2X324/LY-CoV1404 epitope are indicated with arrows.

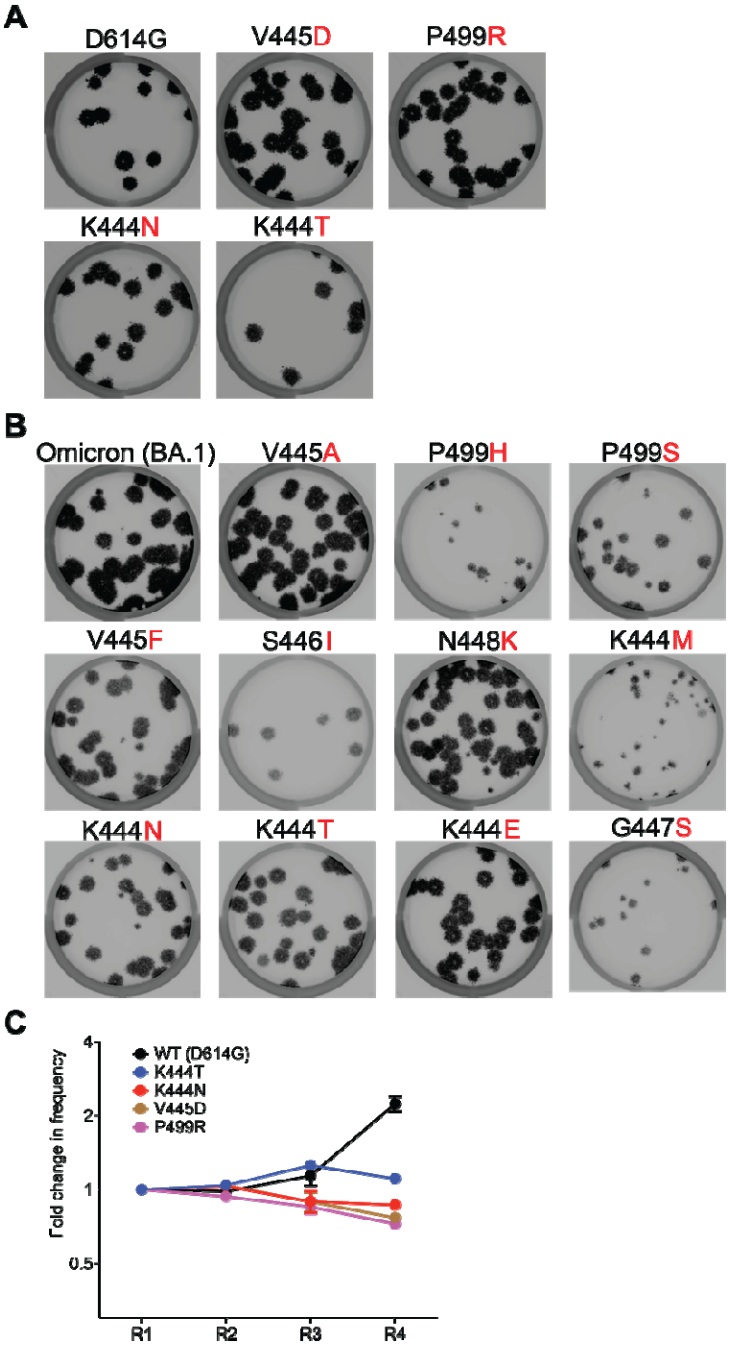

Fig. S15. S2X324 escape clone selection by plaque assays using VSV-SARS-CoV-2 Wuhan-Hu-1 D614G and Omicron BA.1 S chimeric viruses. (A-B) Plaque assays performed to validate the VSV- SARS-CoV-2 S G614 and Omicron BA.1 mutant in Vero cells in the presence (+) of S2X324 in the overlay. (**C**) Replication fitness of S2X324 escape mutations identified in A on Vero E6 cells.

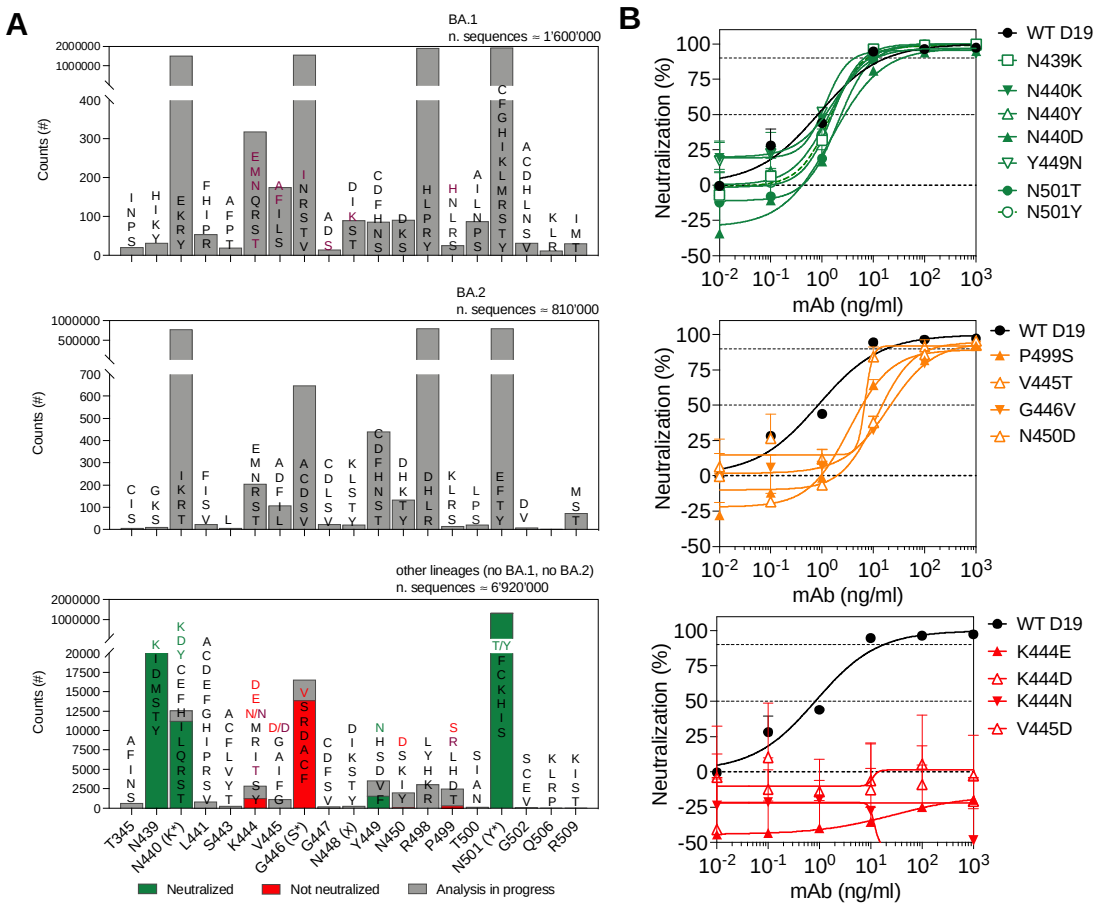

Fig. S16. Counts of observed mutants in S2X324 epitope among SARS-CoV-2 sequences. (**A**) Mutants within the S2X324 epitope on the basis of SARS-CoV-2 variant genome sequences available on GISAID as of 11 April 2022. Colored are shown the mutants neutralized (green) or not neutralized (red) by S2X324 and the escape mutants found with VSV chimera (purple). (**B**) Neutralization against VSV pseudoviruses bearing Wuhan-Hu-1/G614 spike with mutations within the epitope of S2X324.

Table S1. Neutralizing geometric mean titers (GMTs) against Wu-G614, Delta, BA.1, BA.2, and SARS-CoV S VSV pseudoviruses using plasma from subjects who were infected prior to being vaccinated with 2 doses (n=15) or 3 doses (n=8), subjects who experienced a Delta breakthrough infection with 2 doses (n=15), a BA.1 breakthrough infection with either 2 (n=8) or 3 doses (n=8), or were vaccinated-only with 3 doses (n=7).

GMTs	Infected-Vaccinated (2 doses)	Infected-Vaccinated (3 doses)	Delta Breakthrough (2 doses)	BA.1 Breakthrough (2 doses)	BA.1 Breakthrough (3 doses)	Vaccinated only (3 doses)
Wu-G614	2065	6828	2031	5388	5140	1862
Delta	1398	1909	1033	2778	1927	662
BA.1	576	830	560	4226	4608	426
BA.2	1139	1708	792	2441	2464	531
SARS-CoV	129	378	141	158	163	216

Table S2. Description of the Cohorts of SARS-CoV-2-immune individuals, Related to Figure 1B-C

Sample ID	Gender	Vacc.	Doses	COVID diagnosis	Symptom onset	Sample date	Δ days	Cohort*
VC202	F	Yes	3	Yes	2022-03-24	2022-04-12	19	1
VC203	M	Yes	3	Yes	2022-03-12	2022-04-12	31	1
VC204	F	Yes	2	Yes	2022-01-19	2022-04-12	83	1
VC206	F	Yes	2	Yes	2022-03-15	2022-04-12	28	1
VC207	F	Yes	3	Yes	2022-02-19	2022-04-12	52	1
VC208	M	Yes	2	Yes	2021-12-31	2022-04-12	102	1
VC209	F	Yes	3	Yes	2022-03-29	2022-04-12	14	1
VC205	F	No	0	Yes	2022-01-11	2022-04-12	91	2
VC210	F	No	0	Yes	2022-01-21	2022-04-13	82	2
VC211	M	No	0	Yes	2022-03-09	2022-04-14	36	2
VC201	F	Yes	3	No	NA	2022-04-12	NA	3
HCW102	F	Yes	2	Yes	2020-11-25	2021-05-31	187	3
HCW104	F	Yes	2	Yes	2020-11-28	2021-05-31	184	3
HCW105	F	Yes	2	Yes	2020-12-14	2021-05-31	168	3
HCW107	F	Yes	2	Yes	2020-11-25	2021-05-31	187	3
HCW112	F	Yes	2	Yes	2020-10-19	2021-05-31	224	3
HCW114	F	Yes	2	Yes	2020-10-27	2021-05-31	216	3

HCW116	M	Yes	2	Yes	2020-10-19	2021-05-31	224	3
HCW136	F	Yes	2	Yes	2020-11-18	2021-06-01	195	3
HCW144	F	Yes	2	Yes	2020-12-02	2021-06-01	181	3
HCW145	F	Yes	2	Yes	2020-12-29	2021-06-01	154	3

F, female; M, male. *, 1, Vaccinated and infected with Omicron; 2, Not-vaccinated infected with Omicron; 3, Control pre-Omicron vaccinated

Table S3. Neutralizing activity against Wu-G614, Delta, BA.1, BA.2, BA.5 and SARS-CoV S VSV pseudoviruses using plasma from subjects who experienced breakthrough Omicron infection.

		Neutralization of VSV-SARS-CoV1/2 (reciprocal ID50)						Neutralization of VSV-SARS-CoV1/2 (fold loss vs Wu-Hu-1)						Fold loss of BA.5 vs BA.1
	Donor ID	Wu	BA.1	BA.2	BA.5	Delta	SARS-CoV	Wu	BA.1	BA.2	BA.5	Delta	SARS-CoV	BA.5
Vaccinated	VC201	1053	814	229	154	337	114	1	1	5	7	3	9	5
	VC202	4208	3827	2834	1467	2185	162	1	1	1	3	2	26	3
	VC203	4706	1150	1707	1416	2222	264	1	4	3	3	2	18	1
	VC204	7028	5804	2871	1085	4262	160	1	1	2	6	2	44	5
	VC206	6901	5904	2242	903	2510	100	1	1	3	8	3	69	7
	VC207	17538	1410	1533	916	19167	132	1	12	11	19	1	133	2
	VC208	6829	4333	2276	635	4401	126	1	2	3	11	2	54	7
	VC209	22780	7911	6322	2590	8192	368	1	3	4	9	3	62	3
Non-vacc.	VC205	40	564	140	34	23	145	1	0	0	1	2	0	17
	VC210	<10	20	9	<10	<10	31	NC	NC	NC	NC	NC	NC	-
	VC211	598	7294	1556	662	501	86	1	0	0	1	1	7	11

Shown is the reciprocal of the half-maximum inhibitory dose (ID_{50}). NC, not calculable.

Table S4. Neutralizing activity of sotrovimab against VSV psuedoviruses harboring the SARS-CoV-2 Wuhan-Hu-1 S (D614) with the indicated substitutions.

Amino Acid Substitutions	Geometric neutralization IC50 (ng/ml)	Average fold-change in IC_{50} relative to Wild-Type[a]
S371L, S373P, S375F, D614G[b]	72.25	1.31
S371F, S373P, S375F, D614G[c]	207.48	3.44

[a] Fold change calculated relative to wild-type sequence Wuhan-Hu-1 (YP_009724390.1)

[b] Evaluated in Vero E6 cells

[c] Evaluated in Vero E6-TMPRSS2 cells due to decreased infectivity using Vero E6 cells.

Table S5. Kinetics parameters of S2X324 Fab binding to different RBDs evaluated from SPR binding assay with 2 replicates.

Replicate 1								
RBD	**ka (1/Ms)**	**kd (1/s)**	**KD (M)**	**KD (nM)**	**Rmax (RU)**	**tc**	**Chi² (RU²)**	**U-value**
WT	6.92E+05	2.10E-04	3.04E-10	0.30	90.94	7.52E+14	0.175	1
Omicron BA.1	1.89E+05	2.90E-03	1.54E-08	15.37	108.30	1.32E+16	1.56	1
Omicron BA.2	2.79E+05	1.52E-04	5.43E-10	0.54	87.88	3.57E+16	1.62	2

Replicate 2								
RBD	**ka (1/Ms)**	**kd (1/s)**	**KD (M)**	**KD (nM)**	**Rmax (RU)**	**tc**	**Chi² (RU²)**	**U-value**
WT	6.80E+05	2.31E-04	3.39E-10	0.34	85.04	6.41E+14	0.676	1
BA.1	1.78E+05	0.002789	1.57E-08	15.71	129.6	1.43E+09	1.32	1
BA.2	2.52E+05	2.00E-04	7.94E-10	0.79	63.87	3.12E+16	1.45	2

Table S6. CryoEM data collection and refinement statistics.

	SARS-CoV-2 S/S2X324 PDB EMD	SARS-CoV-2 S/S2x324 (local refinement) PDB EMD
Data collection and processing		
Magnification	105,000	105,000
Voltage (kV)	300	300
Electron exposure (e^{-}/Å^2)	60	60
Defocus range (μm)	0.5-2.5	0.5-2.5
Pixel size (Å)	0.843	0.843
Symmetry imposed	C1	C1
Final particle images (no.)	537,649	354,249
Map resolution (Å)	3.1	3.3
FSC threshold	0.143	0.143
Map sharpening *B* factor (Å^2)	-103	-100
Validation		
MolProbity score	1.49	2.03
Clashscore	3.71	5.22
Poor rotamers (%)	0.51	0.82
Ramachandran plot		
Favored (%)	95.2	96.2
Allowed (%)	3.82	3.28
Disallowed (%)	0.92	0.52

Table S7. Summary of nucleotide and amino acid mutations found in neutralization-resistant VSV-SARS-CoV-2 G614 S chimera plaques.

mAb	Clones	Nucleotide mutant	Amino acid mutant
S2X324	#1	G1332T	K444N
	#2	G1332T	K444N
	#3	T133AT	V445D
	#4	C1496G	P499R
	#5	G1332T	K444N
	#6	A1331C	K444T

Table S8. Summary of nucleotide and amino acid mutations found in neutralization-resistant VSV-SARS-CoV-2 Omicron BA.1 S chimera plaques.

mAbs	Clones	Nucleotide mutant	Amino acid mutant
S2X324	#1	G1332T	K444N
	#2	A1330G	K444E
	#3	G1332T	K444N
	#4	C1495T	P499S
	#5	G1332T	K444N
	#6	C1495T	P499S
	#7	T1334C	V445A
	#8	G1332T	K444N
	#9	C1496A	P499H
	#10	A1072T/ T1344C	I358F/ N448K
	#11	C1495T	P499S
	#12	A1330G	K444E
	#13	G1333T	V445F
	#14	G1337T	G446S S446I
	#15	G1332T	K444N
	#16	C1495T	P499S
	#17	T1344C	N448K
	#18	A1331T	N444M
	#19	G1332T	K444N
	#20	A1331C	K444T
	#21	A1331C	K444T
	#22	A1330G	K444E
	#23	G1339A	G447S
	#24	G1332T	K444N

Table S9. Summary of the mutations retrieved from resistance studies with VSV chimera and their prevalence among Delta and Omicron isolates.

	VSV chimera	Delta*	Omicron*	All*
K444N	Wuhan/BA.1	950	96	1,303
K444T	Wuhan/BA.1	103	157	265

K444E	BA.1	20	9	37
K444M	BA.1	144	10	174
V445A	BA.1	217	192	613
V445F	BA.1	246	46	368
V445D	Wuhan	8	40	61
S446I	BA.1	1	22	23
G447S	BA.1	34	10	81
N448K	BA.1	13	3	31
P499H	BA.1	64	13	116
P499R	Wuhan	1,581	12	1,643
		3381	610	4,715
		4,146,647	3,121,074	9,756,845
		0.082%	0.020%	0.048%

*Counts retrieved from GISAID as of May 3, 2022, (sequences with Ns>5% were excluded from analysis)

Table S10. Neutralization against VSV pseudoviruses bearing Wuhan-Hu-1/G614 spike with mutations within the epitope of S2X324.

	IC50 (ng/mL)	FC to Wuhan (D614)
WT	0.83	
N439K	1.60	1.9
N440K	1.16	1.4
N440Y	1.39	1.7
N440D	2.79	3.3
K444E	>1000	>1203.5
K444D	>1000	>1203.5
K444N	>1000	>1203.5
V445D	>1000	>1203.5
V445T	14.87	17.9
G446V	21.47	25.8
Y449N	0.96	1.1
N450D	6.75	8.1
P499S	6.06	7.3
N501Y	1.52	1.8